Wang, Qichang ; Miller, Jimmie ; Von Freyberg, Axel ; Steffens, Norbert ; Fischer, Andreas ; Goch, Gert

Error mapping of rotary tables in 4-axis measuring devices using a ball plate artifact

Journal Article as: peer-reviewed accepted version (Postprint)

DOI of this document*(secondary publication): https://doi.org/10.26092/elib/3314

Publication date of this document: 13/09/2024

* for better findability or for reliable citation

Recommended Citation (primary publication/Version of Record) incl. DOI:

Qichang Wang, Jimmie Miller, Axel Von Freyberg, Norbert Steffens, Andreas Fischer, Gert Goch,
Error mapping of rotary tables in 4-axis measuring devices using a ball plate artifact,
CIRP Annals, Volume 67, Issue 1, 2018, Pages 559-562, ISSN 0007-8506,
https://doi.org/10.1016/j.cirp.2018.04.005.

Error mapping of rotary tables in 4-axis measuring devices using a ball plate artifact

Qichang Wang [a,*], Jimmie Miller [a], Axel Von Freyberg [b], Norbert Steffens [c], Andreas Fischer [b], Gert Goch (1)[a]

[a] University of North Carolina at Charlotte, USA
[b] University of Bremen, Germany
[c] Hexagon Manufacturing Intelligence, Germany

Keywords:
Coordinate measuring machine (CMM)
Compensation
Rotary table

1. Introduction

4-axis measuring devices including coordinate measuring machines (CMM), gear measuring instruments (GMI), form testers, etc. are versatile instruments, used for geometry measurements. As key components, the rotary tables (Fig. 1(a)) provide a quick rotary positioning of components to assess measurands.

Although the performance of rotary tables has been improved dramatically by numerous efforts in design and production, there still exist non-trivial and undesired error motions, originating from the drive train, bearings, rotary encoder, etc.

Compared with mature error mapping techniques for three-axis measuring devices, error determination and compensation of rotary tables are still under development. In many cases, only the angular positioning deviation is corrected by the instrument manufacturers.

To calibrate all six error motions [1] (Fig. 1(b)), the classic method requires a rather sophisticated setup, which includes precision spheres, a polygonal mirror, LVDTs and an autocollimator [2]. A double ball-bar [3–5] is used to calibrate the two tilt error motions and the three translational error motions of the B- and C-axes in 5-axis CNC machines. Another promising method takes advantage of an existing 3-axis measuring device and uses a circular ball plate artifact (Fig. 1(c)), which significantly simplifies the measurement setup [6]. However, without effectively separating the error motions from the deviations of the 3-axis measuring device, the calibration uncertainty is not satisfactory.

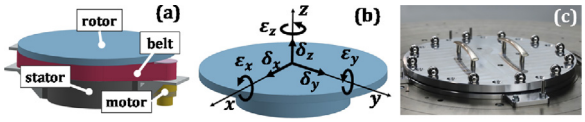

Fig. 1. Error mapping for rotary tables: (a) design schematic (b) six error motions of rotary table, including three translational terms δ_x, δ_y and δ_z, two tilt terms ε_x and ε_y, and one angular positioning deviation ε_z (c) ball plate artifact.

This paper presents a new solution, which completely decouples the error motions of the rotary table from these deviations, originating from the CMM and from the ball plate artifact. Closure theory and approximation techniques are introduced to identify and quantify the error motions, based on obtained point clouds. A mathematical model is developed, which covers all the deviation sources, occurring at the movement of a rotary axis. Simulations and experimental results verify and validate the solution. Based on the mathematical model, this paper presents a new evaluation procedure enabling an error mapping and the corresponding compensation of deviations occurring at rotary tables/axes. The required experimental setup is comparably simple and flexible.

2. Methodology

2.1. Closure theory

Although 3-axis CMMs are flexible and efficient for production metrology, the accuracy even of high-end CMMs is not sufficient to calibrate an artifact. To minimize the CMM's deviations at the

* Corresponding author.
E-mail address: qwang15@uncc.edu (Q. Wang).

measurement of a rotational symmetric artifact with N features (usually spheres), the multiple orientation/measuring technique [7,8] can be applied, based on an N-step repeated measurement. Here, the workpiece is rotated manually by $360°/N$ per step and all features are measured at each step. The angular deviations of the workpiece and CMM can be separated according to the closure theory. In the three-rosette method [8], a rotary table was introduced to rotate the workpiece. The $N \times N$ deviation values were filled into a table with N rows (one for each rotary position) and N columns (one for each sphere). Averaging the rows, columns and diagonals separates the angular deviations of rotary table, workpiece and CMM. The three-rosette method is one option for the calibration of rotary tables.

2.2. Mathematical model

A mathematical model (Fig. 2) was developed for feasibility studies. The measured center (P_m) of a sphere given in the frame coordinate system (CS) is described by Eq. (1). In Eq. (1), the subscripts W, C and F denote the workpiece CS, the rotary table CS and the frame CS, respectively. $[S]_W$ denotes the actual position of a sphere by superimposing the nominal coordinates with deviations. The matrix R_{WC} describes the 3D rotation from the artifact to the rotary table. It contains the artifact's tilt deviations ε_{Ax} and ε_{Ay}. $[H_W]_C = [H_x; H_y; 0]_C$ represents the eccentricity of the artifact's center, relative to the real axis of rotation of the rotary table. The rotation matrix R_{CF} contains the rotary table's tilt error motions ε_x and ε_y, as well as the angular positioning deviation ε_z. The vector $[\Delta C]_F$ consists of the translational error motions δ_x, δ_y and δ_z. $[T_C]_F$ is a vector from the origin of the frame CS to the origin of the rotary table CS.

$$[P_m]_F = R_{CF}([H_W]_C + R_{WC}[S]_W) + [\Delta C]_F + [T_C]_F + [\Delta P_s]_F + [\Delta P_r]_F + [\boldsymbol{\Delta} P_p]_F \quad (1)$$

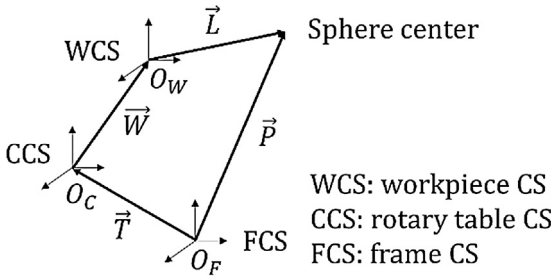

Fig. 2. Developed mathematical vector model illustrating the chain coordinate system (CS) from the frame CS (CMM) to the sphere center.

Error mapping of a rotary table requires a sufficient sample density per cycle. Therefore, the angular step is reduced to $360°/M$. M is a multiple of N, which denotes the number of spheres. After one complete rotation of the ball plate, each of the N spheres has been positioned once near each of the M defined measuring positions. The CMM's deviations in this mathematic model can be simplified significantly. The required efforts in terms of both manufacturing of the artifact and experimental setup are limited: (1) the radial, pitch and axial deviations of each sphere of the ball plate should be less than 100 μm [9]; (2) the artifact should be centered on the table within 100 μm range. In this case, the $M \times N$ sphere centers are within 1 mm range around the corresponding measuring positions. Consequently, it appears reasonable to assume that the CMM's systematic deviations are constant within this range around one ideal measuring position, where N different spheres centers were measured. In that case, the superimposed deviations of the probing system and 21 deviations of CMM guideways are replaced by three vectors: $[\Delta P_s]$, $[\Delta P_r]$ and $[\Delta P_p]$. $[\Delta P_s]$ denotes the systematic deviations and $[\Delta P_r]$ denotes the stochastic deviations, respectively, of length measurement from the artifact center to one sphere center. $[\Delta P_p]$ represents the non-repeatable deviations of the sphere center, originating from the probing deviations.

Based on Eq. (1), pure formula derivations following the three-rosette method were carried out. Three tables were used for error calculations in radial, angular and axial directions, leading to several results, which did not fully meet the goals stated in Section 1. The major deficit was that not all the error motions and deviations originating from the rotary table, the CMM and the ball plate could be separated satisfactorily without additional assumptions or experimental restrictions. Therefore, within the approach presented here, the three-rosette method is used to determine the CMM's systematic deviations and to find reasonable starting values for the approximation algorithm (Section 2.3).

2.3. New solution

Based on this mathematical model (Section 2.2), a new solution is proposed to separate the six error motions of rotary table from the ball plate deviations and the CMM's systematic deviations. In the first step, the CMM's systematic deviations $[\Delta P_s] = [\Delta P_{sa}; \Delta P_{sr}; \Delta P_{sz}]$ at each measuring position are separated with the three-rosette method. The subscripts a, r and z denote the angular, radial and axial directions, respectively. Then, the measured data is corrected using these systematic deviations of the CMM. The non-repeatable deviations $[\Delta P_r] = [\Delta P_{ra}; \Delta P_{rr}; \Delta P_{rz}]$ and $[\Delta P_p] = [\Delta P_{pa}; \Delta P_{pr}; \Delta P_{pz}]$ are minimized later.

In the second step, since the deviations of the artifact in angular and axial direction follow the closure theory, the rotary table's error motions δ_z and ε_z are determined by the three-rosette method as well. The order of the first two steps cannot be reversed.

In the third step, the artifact center is tracked to determine the error motions δ_x. Because δ_x is periodic, one trigonometric polynomial [10] (Eq. (2)) is approximated to the movement of the artifact center along the x-axis. The first order terms $a_{1.c}$ and $a_{1.s}$ give the eccentricity of the artifact, while the other terms $a_{m.c}$, $a_{m.s}$, $a_{n.c}$ and $a_{n.s}$, with $m \geq 2$ and $n \geq 2$, denotes the coefficients of the trigonometric terms for δ_x. The approximation technique delivers three partial solutions at once: determining the unknown eccentricity of the artifact; generating an error map; minimizing the influence of the non-repeatable deviations of the CMM. δ_y is determined in the same way. In the fourth step, a similar approach determines the tilt error motions ε_x and ε_y, based on a least squares approximation of the artifact's normal direction (perpendicular to the plane formed by the spheres).

$$poly = \sum_{m=1}^{N_1} [a_{m.c}\cos(m\theta) + a_{m.s}\sin(m\theta)] + \sum_{n=2}^{N_2} \left[a_{n.c}\cos\left(\frac{\theta}{n}\right) + a_{n.s}\sin\left(\frac{\theta}{n}\right)\right] \quad (2)$$

3. Numerical simulation

Numerical simulations were performed based on the mathematical model to verify the proposed solution. Simulated data of sphere centers was generated with given deviation values of the CMM, rotary table and artifact. Then, the simulated data was processed to separate the deviations from different sources.

3.1. Simulation inputs

The input values of a circular ball plate (Ø 400.0 mm) with 12 spheres (Ø 30.0 mm) are described in Fig. 3 and Table 1. By selecting $M = 48$ (see Section 2.2), the angular step of ball plate's rotation was 7.5° for three continuous cycles. The systematic components of the vector $[\Delta P_s]$ were selected randomly from the interval $0.5 \times [-E_{L,MPE} + R_{0,MPL}, E_{L,MPE} - R_{0,MPL}]$, while the statistic components of the vector $[\Delta P_r]$ followed Gaussian distributions within $0.5 \times [-R_{0,MPL}, R_{0,MPL}]$. E_L denotes length measurement error, while the subscript MPE stands for maximum permissible

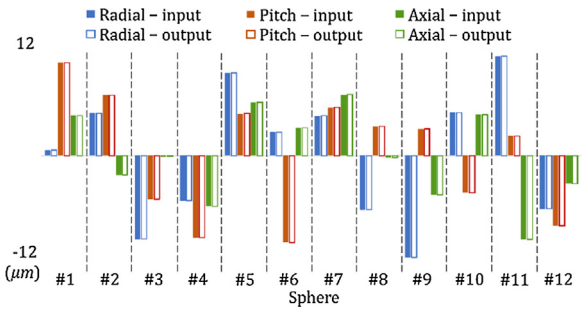

Fig. 3. Simulation inputs and outputs of sphere position deviations.

Table 1
Simulated deviations of the ball plate artifact.

Deviation	Parameter	Input	Output	Residual
Eccentricity	H_x	24.000 μm	23.996 μm	−0.004 μm
	H_y	−18.000 μm	−17.992 μm	0.008 μm
Tilt	ε_{Ax}	1.023″	1.017″	−0.006″
	ε_{Ay}	6.460″	6.461″	0.001″

error [11]. R_0 denotes the repeatability range of length measurement, while the subscript MPL standards for the maximum permissible limit. $E_{L,MPE} = (1.8 + L/500)$ μm and $R_{0,MPL} = 0.6$ μm were obtained from the data sheet of a Leitz CMM. The statistic component $[\Delta P_p]$ followed a random distribution within ±0.15 μm, assuming that the sphere center is calculated by probing 15 points on one sphere [12]. Systematic error motions of the rotary table had spectral components up to the eighth order. Other key inputs can be found in Section 3.2.

3.2. Simulation results

First, the CMM's systematic deviations at 48 measuring positions were separated, as interpreted in Fig. 4. The residuals primarily resulted from statistic components of the deviations $[\Delta P_r]$ and $[\Delta P_p]$. After correcting the simulated data by the CMM's systematic deviations, the error motions of the rotary table were determined (Fig. 5). Trigonometric polynomials were approximated to data from 3 full cycles to ascertain the error motions in one cycle. The simulation outputs (yellow dots) matched the corresponding inputs (blue solid curves) very well. Angular steps of 7.5° seem to be sufficient to characterize the input error motions. The maximum residuals were not larger than 0.04 μm for the translational error motions and 0.03″ for the tilt and angular positioning error motions.

Compared with its nominal position, each sphere usually shows a two-digit micrometer deviation. This primarily resulted from two groups of sources: (i) imperfect fabrication of base plate and assembly of the artifact; (ii) clamping force and imperfect centering of the artifact. Deviations of the first type can be predetermined by using a more accurate measuring device. Deviations of the second type can only be determined in situ, but even a

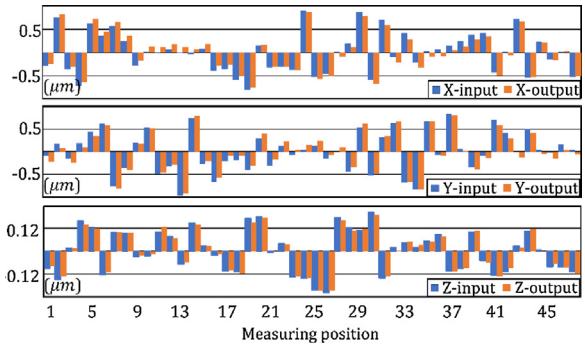

Fig. 4. Simulation inputs and outputs of the CMM's systematic deviations along the x-, y- and z-axes at the 48 measuring positions.

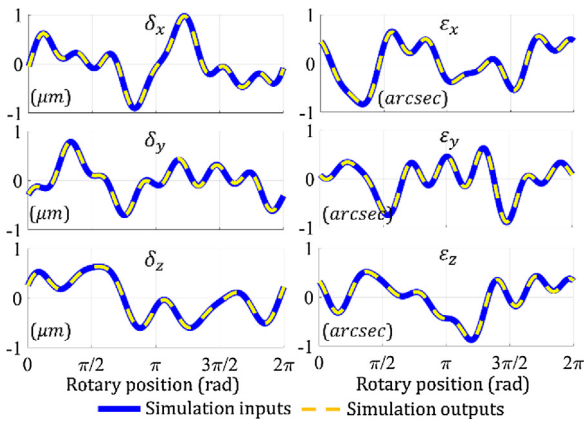

Fig. 5. Simulation inputs and outputs of the rotary table's error motions.

high-end 3-axis CMM is not sufficient to accomplish the task alone. The three-rosette method is a good option, since the CMM's systematic deviations are neutralized. The proposed solution also decouples the eccentricity of the artifact (Table 1) from the radial and angular position deviations of spheres. Therefore, a very precise centering of the artifact is not necessary.

4. Experiments

Experiments were conducted at the UNC Charlotte and at the University of Bremen to calibrate an aerostatic and a hydrostatic rotary table, respectively.

4.1. Experimental setup

Experiments (Fig. 6(a)) at the UNC Charlotte used a Leitz PMM-F, an aerostatic rotary table and a stacked double-plate artifact (Ø 400.0 mm, 12 spheres) (Fig. 6(b)). The lower plate functioned as a base layer to isolate clamping forces. Therefore, the upper plate was freed from the resulting distortion. The outer cylindrical surface assisted the centering of the lower plate. Maxwell kinematic coupling allowed the full constraint and a quick alignment of the upper plate. Countersinks reduced the position deviations of spheres due to assembly. Spheres were secured on the plate with short pins and 5-min epoxy.

Once fabricated and assembled, the double-plate artifact was centered and fixed on the rotary table. Stability of the artifact (especially curing of the glue) was monitored by measuring the coordinates of all the spheres continuously (the table was at stationary condition). After one week, the coordinates of every sphere varied within ±0.2 μm in a period of 24 h, indicating that the artifact reached an equilibrium status. The artifact's temperature drift was less than 0.1 °C in the same period. The result also revealed that the CMM had constant systematic deviations at the positions of 12 spheres and low non-repeatable deviations of length measurement.

Experiments (Fig. 7(b)) at the University of Bremen used a Leitz PMM-F, a hydrostatic rotary table and a single-plate artifact (Ø 200.0 mm). The artifact also reached the equilibrium status before the experiments.

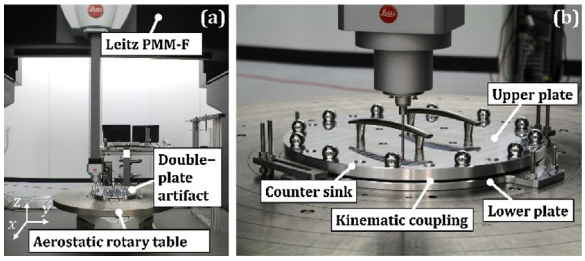

Fig. 6. Experimental setup at the UNC Charlotte: (a) entire system (b) double-plate artifact.

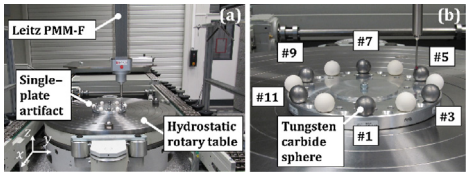

Fig. 7. Experimental setup at the University of Bremen: (a) entire system (b) artifact, where the six tungsten carbide spheres were measured.

4.2. Calibration procedure

The same experimental procedures were conducted in both laboratories. After a warm-up routine, the rotary table was rotated by multiple cycles in the counter-clockwise (CCW) direction in steps of 7.5° (M = 48). At each step, 15 points were taken on each of the #1, #3, #5, #7, #9, #11 spheres (N = 6).

The determined CMM's deviations at the 48 measuring positions are presented in Fig. 8. Small discrepancy in multiple cycles proved the consistent performance of both CMMs.

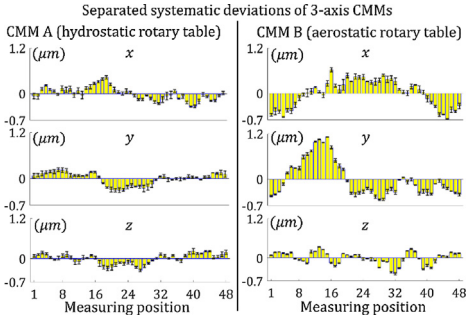

Fig. 8. Determined systematic deviations of the two CMMs at the 48 measuring positions. CMM A represent the CMM for the hydrostatic rotary table and CMM B refers to the other one for the aerostatic rotary table.

4.3. Experimental results: hydrostatic rotary table

Fig. 9 shows the separated six error motions at sampled rotary positions, when the table was rotated in three continuous cycles. δ_x had a period of 2π, which matches the characteristic of rotary tables employing external-pressurized bearing systems like hydrostatic bearings. The maximum deviation of 0.17 μm in three cycles reflects the stable performance of the rotary table. Similar phenomena were observed for δ_y, ε_x, ε_y and ε_z. However, δ_Z did not have a fully repeatable pattern in multiple cycles, which may result from the thickness variation of the thin oil film employed by the hydrostatic bearing. It is much more difficult to control the temperature of a hydrostatic bearing than the one of an aerostatic bearing, because the heat generated in the bearing cannot be dissipated easily in such an enclosed system. Nevertheless, the peak amplitude of 0.3 μm will have a minor effect in most applications of production metrology.

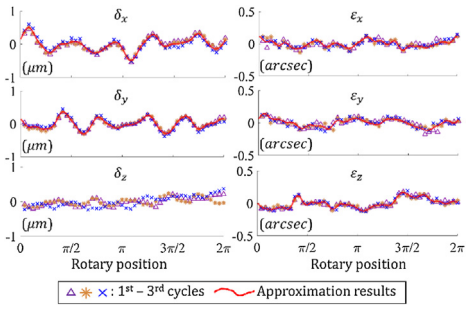

Fig. 9. Separated six error motions of a hydrostatic rotary table in three cycles.

4.4. Experimental results: aerostatic rotary table

The δ_z of the aerostatic rotary table had a maximum deviation of 0.07 μm in two cycles, which matches the discussion in Section 4.3. The δ_x had a non-integer period (around 1.8π). Therefore, this plot was left out in Fig. 10, because the superposition of two non-periodic cycles would give a confusing image. The non-integer period may result from the drive and transmission trains. The tilt error motions ε_x and ε_y and the angular positioning deviation ε_z were less than $\pm 0.15''$ for both rotary tables, which is satisfactory.

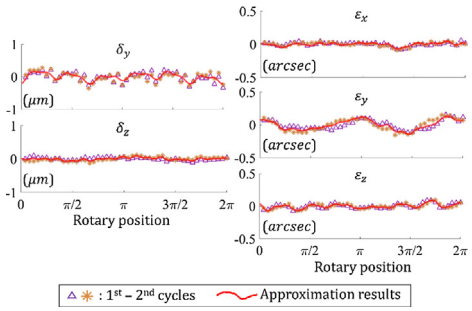

Fig. 10. Separated error motions (except δ_x) of an aerostatic rotary table in two cycles.

Summary and future work

This paper presents a new error mapping solution, which decouples the error motions of the rotary table/axis from the deviations originating from the CMM and from the ball plate artifact. The closure theory and approximation techniques are introduced. A mathematical model is developed. Simulations and experimental results verify the solution. It is promising to apply this solution for error mapping in production metrology. Future work will include investigations in both rotating directions (CCW and CW) as well as influences of load conditions (varying workpiece masses, eccentric clamping) on the error motions.

Acknowledgments

The authors gratefully acknowledge the financial support by the Center for Precision Metrology at UNC Charlotte. The authors also thank Mr. Jesse Groover, Dr. Kang Ni, Ms. Yue Peng and Mr. Frank Horn for their help and insightful discussions.

References

[1] ISO 230-7:2015, Test Code for Machine Tools — Part 7: Geometric Accuracy of Axes of Rotation.
[2] Suh SH, Lee ES, Jung SY (1998) Error Modelling and Measurement for the Rotary Table of Five-axis Machine Tools. *The International Journal of Advanced Manufacturing Technology* 14(9):656–663.
[3] Lei WT, Sung MP, Liu WL, Chuang YC (2007) Double Ballbar Test for the Rotary Axes of Five-axis CNC Machine Tools. *International Journal of Machine Tools and Manufacture* 47(2):273–285.
[4] Zhang Y, Yang J, Zhang K (2013) Geometric Error Measurement and Compensation for the Rotary Table of Five-axis Machine Tool with Double Ballbar. *The International Journal of Advanced Manufacturing Technology* 1–7.
[5] Ibaraki S, Knapp W (2012) Indirect Measurement of Volumetric Accuracy for Three-axis and Five-axis Machine Tools. *International Journal of Automation Technology* 6(2):110–124.
[6] Kunzmann H, Schepperle K, Trieb G, Waldele F, Carl-Zeiss-Stiftung (1989) Method of Measuring Rotary-table Deviations, U. S. patent US4,819,339.
[7] Osawa S, Busch K, Franke M, Schwenke H (2005) Multiple Orientation Technique for the Calibration of Cylindrical Workpieces on CMMs. *Precision Engineering* 29(1):56–64.
[8] Kniel K, Härtig F, Osawa S, Sato O (2009) Two Highly Accurate Methods for Pitch Calibration. *Measurement Science and Technology* 20(11):115110.
[9] Guenther A, Stöbener D, Goch G (2016) Self-calibration Method for a Ball Plate Artefact on a CMM. *Annals of the CIRP* 65(1):503–506.
[10] Miller J (2016) Two-dimensional Matrix-based Non-complex Axis-of-rotation Error Modelling. *Precision Engineering* 44:93–108.
[11] ISO 10360-2:2009, Acceptance and Reverification Tests for Coordinate Measuring Machines — Part 2: CMMs Used for Measuring Linear Dimension.
[12] ISO 10360-5:2010, Acceptance and Reverification Tests for Coordinate Measuring Machines — Part 5: CMMs Using Single and Multiple Stylus Contacting Probing Systems.